RECENT PROGRESS IN THE GROWTH OF MID-INFRARED EMITTERS BY METAL-ORGANIC CHEMICAL VAPOR DEPOSITION

R. M. Biefeld, A. A. Allerman, S. R. Kurtz, and K. C. Baucom
Sandia National Laboratory, Albuquerque, New Mexico, 87185, USA

ABSTRACT

We report on recent progress and improvements in the metal-organic chemical vapor deposition (MOCVD) growth of mid-infrared lasers and using a high speed rotating disk reactor (RDR). The devices contain AlAsSb claddings and strained InAsSb active regions. These lasers have multi-stage, type I InAsSb/InAsP quantum well active regions. A semi-metal GaAsSb/InAs layer acts as an internal electron source for the multi-stage injection lasers and AlAsSb is an electron confinement layer. These structures are the first MOCVD multi-stage devices. Growth in an RDR was necessary to avoid the previously observed Al memory effects found in conventional horizontal reactors. A single stage, optically pumped laser yielded improved power (> 650 mW/facet) at 80 K and 3.8 μm. A multi-stage 3.8-3.9 μm laser structure operated up to T=170 K. At 80 K, peak power > 100 mW and a high slope-efficiency were observed in gain guided lasers.

INTRODUCTION

Mid-infrared (3-6 μm) lasers and LEDs are being developed for use in chemical sensor systems and infrared countermeasure technologies. These applications require relatively high power, mid-infrared lasers and LEDs operating near room temperature. The radiative performance of mid-infrared emitters has been limited by nonradiative recombination processes (usually Auger recombination) in narrow bandgap semiconductors. Potentially, Auger recombination can be suppressed in "band-structure engineered", strained Sb-based heterostructures. We have demonstrated improved performance for midwave infrared emitters in strained InAsSb heterostructures due to their unique electronic properties that are beneficial to the performance of these devices.[1-3] To further improve laser and LED performance, we are exploring the MOCVD-growth of novel multi-stage (or "cascaded") active regions in InAsSb-based devices.

Multi-stage, mid-infrared gain regions have been proposed for several material systems.[1-6] Ideally, a laser with an N-stage active region could produce N photons for each carrier injected from the external power supply. Thereby, multi-staging of the laser active region may increase gain, lower threshold current, and finally increase the operating temperature of gain-limited, mid-infrared lasers. The success of the unipolar, quantum cascade laser demonstrates the benefit of multi-stage gain regions.[7] However, the nonradiative (optical phonon) lifetimes of the unipolar devices are orders of magnitude shorter than the Auger-limited lifetimes for interband devices, and with multi-staging, mid-infrared interband Sb-based lasers may have lower threshold currents than unipolar quantum cascade lasers.

Gain regions with multiple electron-hole recombination stages have been proposed for Sb-based lasers.[1,5,6] These devices utilize a semimetal layer, formed by an InAs (n) / GaAsSb (p) heterojunction, as an internal electron-hole source between stages. Recently, cascaded lasers with type II InAs/GaInSb active regions have been demonstrated.[8] The type II lasers were grown by molecular beam epitaxy, and characteristic of multi-stage lasers, large differential quantum efficiencies (> 1) are now reported.[9] In this work we demonstrate 10-stage lasers composed of InAsSb quantum wells with type I band offsets.

A band diagram of our multi-stage active region, under forward bias, is shown in Figure 1. Electron-hole recombination occurs in compressively strained InAsSb quantum wells separated by tensile strained InAsP barriers. The type I, InAsSb/InAsP quantum wells have a large light-heavy hole splitting required for suppression of Auger recombination.[2] Electron-hole pairs for each stage are generated at a semi-metal, GaAsSb (p)/ InAs (n) heterojunction. An AlAsSb layer prevents electrons from escaping; nominal hole confinement is provided by the InAsSb quantum well valence band offset relative to the InAsP barrier layer in this initial device. Ideally, electron-hole generation replenishes the carriers which recombine in each stage, and for each carrier injected

DISCLAIMER

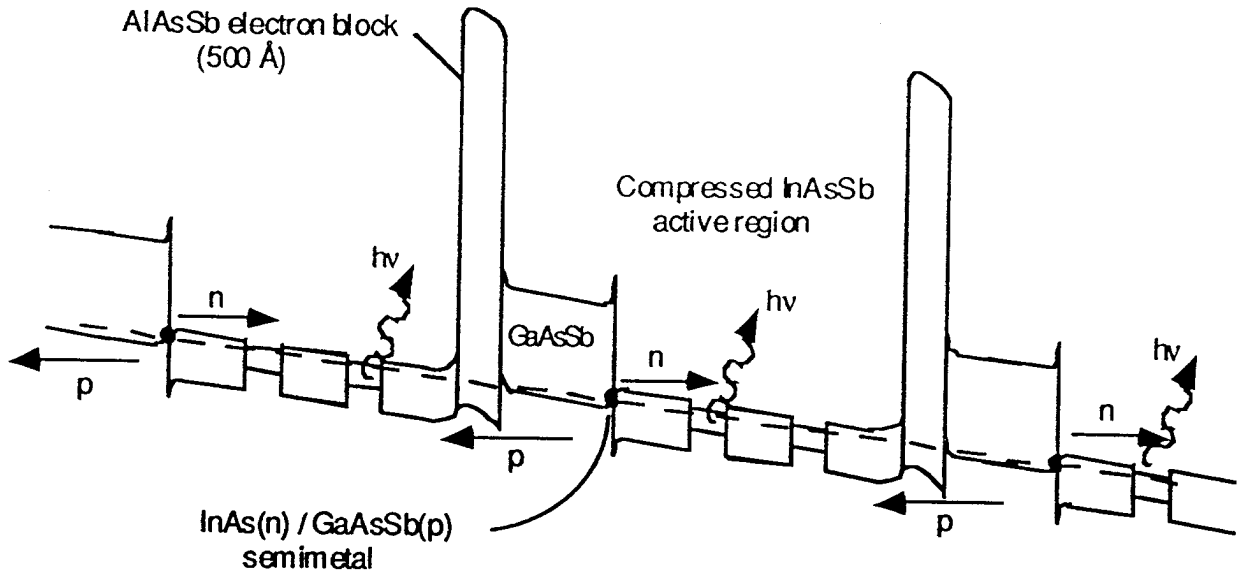

Figure 1 - Band diagram of a multi-stage laser active region with compressed, type I InAsSb quantum wells separated by InAsP barriers, electron-hole generation by an InAs(n)/GaAsSb(p) semimetal heterojunction, and an AlAsSb electron block

from the external circuit, the multi-stage active region can emit several photons resulting in an overall quantum efficiency greater than unity. In practice, charge can accumulate in the active region, shift the Fermi-level, and turn-off electron generation at the semi-metal. Previously, we have found that a AlGaAsSb graded layer between the AlAsSb and GaAsSb layers reduces hole trapping, thus increasing laser duty cycles and lowering turn-on voltages.

Unlike previous cascaded lasers, our device was grown by metal-organic chemical vapor deposition (MOCVD). Our devices are among the most complex structures ever grown by MOCVD, and it can be difficult to alternate Al, In, Ga, P, As, or Sb bearing materials while maintaining sharp interfaces and not having chemical carry-over into other layers. In particular, we have found that the combination of novel Al organometallic sources and an MOCVD, vertical, high speed rotating-disk reactor (RDR) is necessary to grow these structures to avoid the chemical carry-over previously observed with a horizontal reactor.[3] Even with an RDR, it is necessary to optimize the growth conditions and the reactor configuration as discussed below to minimize the effects of chemical carry over.

EXPERIMENTAL

This work was carried out in a previously described vertical, high-speed, rotating-disk reactor (RDR).[10] Ethyldimethylamine alane (EDMAA), trimethylindium (TMIn), triethylgallium (TEGa), triethylantimony (TESb) , diethylzinc (DEZn), phosphine, and tertiarybutylarsine (TBAs) or arsine were used as sources. P-type doping was accomplished using diethylzinc (DEZn) in a dilution system. The structures were grown at 500 ^{0}C and 70 torr. The V/III ratios were optimized separately for each material and the InAsSb/InAsP strained-layer superlattice. The growth was performed on (001) InAs substrates. Hydrogen was used as the carrier gas at a flow of 18.5 slpm with a substrate rotation speed of 1500 rpm to retain matched flow conditions.[10] Semi-insulating, epi-ready GaAs or n-type InAs substrates were used for each growth.

Both InAsSb/InAs and InAsP/InAs multiple quantum wells (MQWs) were grown by MOCVD on n-type InAs substrates for calibration purposes to determine the solid-vapor distribution coefficients separately for Sb in InAsSb and P in InAsP. The InAsSb/InAsP SLSs were lattice matched to InAs with $\Delta a/a < 0.0004$. The MQW and SLS composition and strain were determined by double crystal x-ray diffraction.

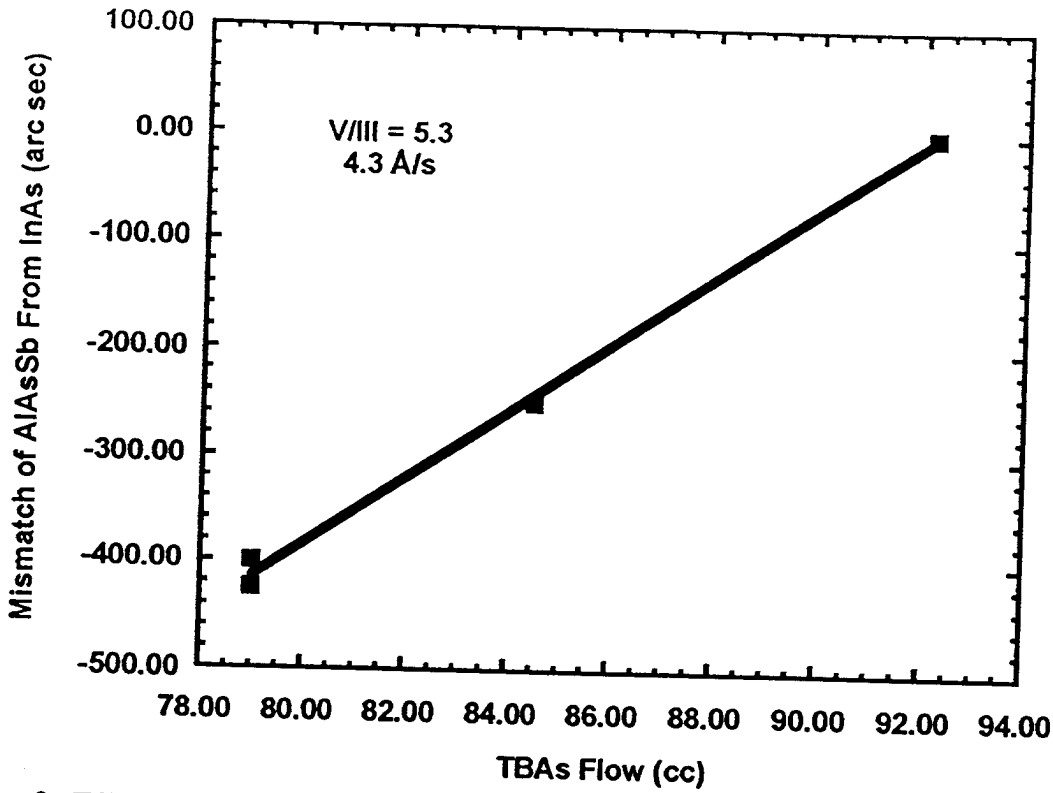

Figure 2. Effect of change in TBAs flow on the lattice match to the InAs substrate of an AlAsSb layer grown at 500 °C, 70 torr, a V/III ratio of 5.3, and a growth rate of 4.3 Å/s.

Double crystal x-ray diffraction (DCXRD) of the (004) reflection was used to determine alloy composition and layer thicknesses. Layer thicknesses were also determined using a groove technique and these were checked in several instances by cross sectional SEM. These techniques usually agreed within a few percent.

Infrared photoluminescence (PL) was measured on all samples from 14 K up to 300 K using a double-modulation, Fourier-transform infrared (FTIR) technique which provides high sensitivity, reduces sample heating, and eliminates the blackbody background from infrared emission spectra. Injection devices also were characterized with double modulation FTIR.

RESULTS AND DISCUSSION

MOCVD Growth

The optimum growth conditions for $AlAs_xSb_{1-x}$ occurred at 500 °C and 70 torr at a growth rate of 4.3 Å/s using a V/III ratio of 5.3 assuming a vapor pressure of 0.75 torr for EDMAA at 19.8 °C and an [TESb]/([TBAs]+[TESb]) ratio of 0.83. The growth rate was found to be dependent on the EDMAA flow and independent of the group V flows for the conditions examined in this work. The best surface morphologies with the lowest number of defects were obtained by using a buffer layer grown before the $AlAs_xSb_{1-x}$ layer. The defects consisted primarily of square pyramidal hillocks 10 to 20 μm on a side. Lattice matched $AlAs_xSb_{1-x}$ films of high crystalline quality, as evidenced by double crystal x-ray diffraction (DCXRD) where full widths at half of the maximum intensity (FWHM) of less than 50 arc sec were obtained. Typical InAs substrate peaks

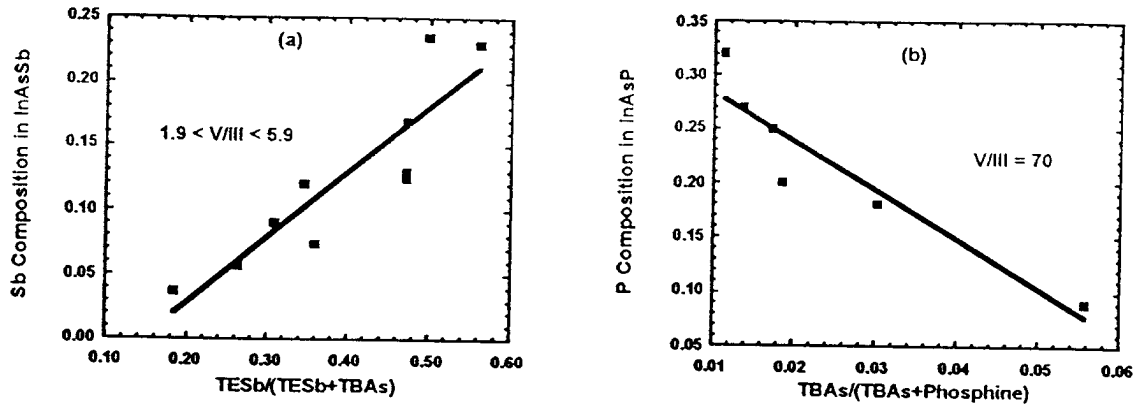

Figure 3. The composition variation of InAsSb and InAsP as a function of vapor phase composition under optimized growth conditions. (a) Dependence of Sb composition on the TESb/(TESb+TBAs) vapor phase composition. (b) Dependence of P composition on the variation of TBAs/(TBAs+Phosphine) vapor phase composition.

were 10-20 arc sec. The x-ray peak width of 50 arc seconds could be due to some variation in composition with growth time as discussed below or to phase separation. We were also able to reproducibly obtain lattice matching of $AlAs_xSb_{1-x}$ to InAs to within less than 0.015 percent using the optimized growth conditions. Figure 2 shows the variation of lattice mismatch from the InAs substrate or composition as a function of TBAs flow for the optimized growth conditions. This variation was reproducible at these growth conditions. Hall measurements of AlAsSb films 1 μm thick with 200Å GaAsSb cap layers grown on GaAs substrates indicated background hole concentrations between 0.5 to 1 $x10^{17}$ cm^{-3}. The residual hole concentration of GaAsSb films on GaAs ranged between 4 to $7x10^{16}$ cm^{-3}. The use of other than the above stated growth conditions led to several significant problems during the growth of $AlAs_xSb_{1-x}$ layers lattice matched to InAs. These included composition control and reproducibility. For instance, growth at higher V/III ratios resulted in a large drift in composition from run to run. Composition variations have also been observed due to excess cooling of the chamber walls, probably due to an Sb memory effect on the inlet to the reactor.

We have successfully doped the $AlAs_xSb_{1-x}$ layers p-type using DEZn. We achieved p-type levels of 1 x 10^{16} to 6 x 10^{17} cm^{-3}. The mobilities for the $AlAs_xSb_{1-x}$ layers ranged from 200 to 50 cm^2/Vs with no clear trend that could be associated with the carrier concentration or type. SIMS measurements on the Zn doped samples indicated a similar level of Zn compared to the p-type carriers indicating complete activation of the Zn.

The growth of InAsSb/InAs and InAsP/InAs MQW structures were examined to optimize the growth of the ternaries. The growth conditions for both of these MQW's were examined at 500 °C and 70 torr using a rotation speed of 1500 rpm and a total H_2 flow of 18.5 SLM to retain matched flow conditions.[10] Growth rates of 2.8 Å/s were used for both systems. The growth rate was found to be proportional to the TMIn flow into the reaction chamber and independent of the group V flows. A purge time of 15 to 20 seconds with arsine flowing during the purge was used between InAs and the ternary layer growth to allow for source flow changes during the growth of the MQWs. Figure 3(a) illustrates the dependence of Sb composition on the TESb/(TESb+TBAs) vapor phase composition for optimized growth conditions. In this set of experiments the flow of TESb was held constant while the TBAs flow was varied to change the Sb solid composition. The V/III ratio varied from 1.9 to 5.9. A low V/III ratio is necessary for the growth of high quality InAsSb due to the low vapor pressure of Sb; excess Sb tends to cause surface morphology defects. In Figure 3(b) the dependence of P composition in InAsP on the variation of TBAs/(TBAs+Phosphine) vapor phase composition is illustrated. The flow of phosphine was held constant and the flow of TBAs was varied. In this case the V/III ratio is dominated by the excess phosphine flow and was approximately constant at 70. The high V/III ratio and excess phosphine,

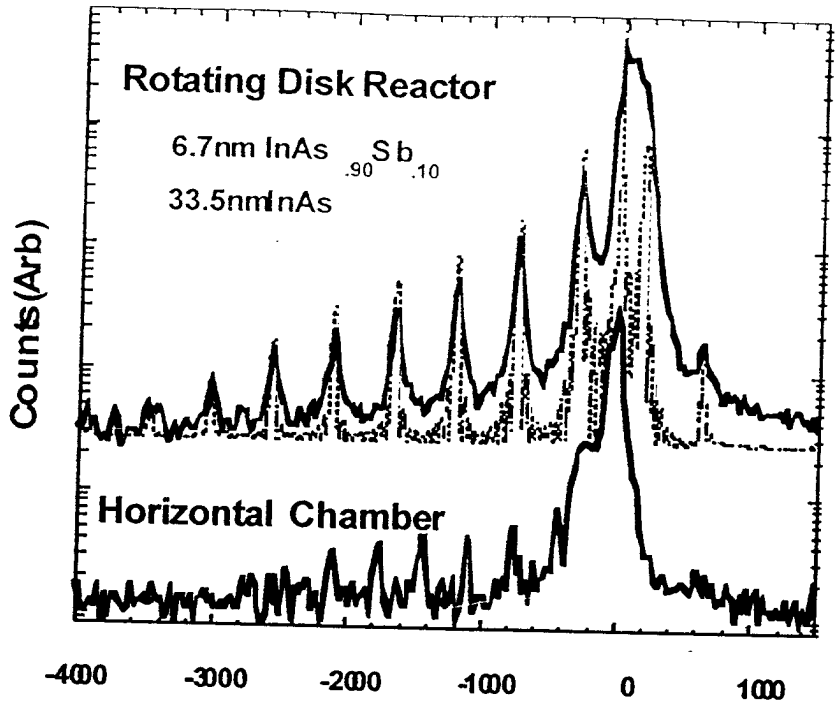

Figure 4. Comparison of the x-ray diffraction pattern of an InAsSb/InAs MQW laser structure grown in an MOCVD RDR(top pattern) versus the pattern for a MQW laser grown using a standard horizontal chamber configuration (bottom). The dotted line is a simulated x-ray spectrum for the RDR grown structure.

flow are necessary because of the high decomposition temperature of phosphine. In both cases, InAsSb/InAs and InAsP/InAs, the composition dependence was reproducible and approximately linear over the composition range that was examined.

Several test laser structures were prepared similar to the one previously reported using InAsSb/InAs MQW active regions.[3] These structures consisted of 2 μm AlAsSb top and bottom cladding layers with InAsSb/InAs 10 period MQW active regions and a (p)-GaAsSb/(n)-InAs semi-metal heterojunction for charge transfer.[1-3] The difference in the quality of the x-ray diffraction pattern of the continuously grown structure from the RDR and the re-grown active region and top cladding is illustrated in Figure 4. The continuously grown structures can be seen to be of much better quality from the x-ray diffraction pattern (top pattern). Similar lasing characteristics were obtained for both the RDR and re-grown structures. The advantage of the RDR growths is that no Al carry-over was observed as was found for the re-grown structures using the horizontal reactor.[3] The multi-staged laser structures described in this paper could not be grown using a conventional horizontal MOCVD system.

The growths of the InAsSb/InAsP ternary strained-layer superlattices (SLSs) used similar conditions as those for the MQW growths. The growth conditions for a given composition of the SLS was easily predicted from the compositions of the MQW's. However, very rough surface morphologies and poor x-ray diffraction patterns and photoluminescence characteristics were found for the 15-20 second purge times used between layers. The purge times were optimized using both x-ray diffraction patterns, as illustrated in Figure 5 for the x-ray diffraction patterns, as well as photoluminescence. As shown in Figure 5(a) and (b) for purge times of 20 and 5 seconds, very broad x-ray diffraction patterns were observed. The x-ray diffraction patterns shown in Figure 5(c) and (d) differ only in composition; both were grown using no purges between layers. The sample in (d) was grown with a slightly different composition to achieve lattice matching with the InAs substrate. The optimized time for the ternary SLS's was found to be less than 5 seconds. Similar characteristics were found for purge times of 0 or 1 second with arsine continuing to flow during the purge times as well as during the growth of the layers.

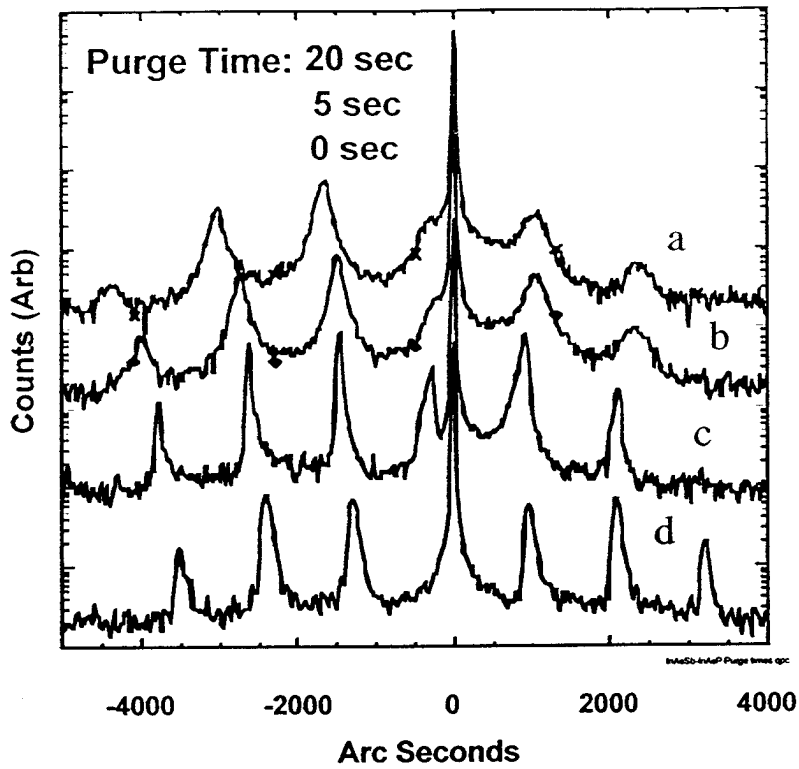

Figure 5. Comparison of the x-ray diffraction patterns for InAsSb/InAsP SLS's grown using identical growth conditions in (a), (b), and (c) but with the indicated purges between layers [(a) = 20 sec., (b) = 5 sec., and (c) = 0 sec.]. The sample in (d) was grown with a slightly different composition than (c) with no purge time to achieve lattice matching with the InAs substrate.

Optically Pumped Laser Design and Characteristics

Several laser structures have been examined by optical pumping in our previous work.[1] These structures consisted of an InAs substrate with a 2.5 μm thick AlAsSb lower cladding, a 1.0 μm thick, $InAs_{0.89}Sb_{0.11}$ /$InAs_{0.77}P_{0.33}$ (83Å / 87Å) SLS active region and several different top terminations. For the limited number of devices studied, neither a top cladding nor a semi-metal injection layer seemed to significantly affect laser performance under optical pumping. The SLS laser was pumped with a Q-switched Nd:YAG (1.06 μm, 20 Hz, 10 nsec pulse, focused to a 200 μm wide line), and emission was detected with an FTIR operated in a step-scan mode. Laser emission was observed from cleaved bars, 1000 μm wide, with uncoated facets. A lasing threshold and spectrally narrowed, laser emission was seen from 80 K through 240 K, the maximum temperature where lasing occurred. At 80 K, peak powers >100 mW could be obtained. The temperature dependence of the SLS laser threshold is described by a characteristic temperature, T_0= 33 K, over the entire range. Similar experiments on structures containing 2000 Å InAs top and bottom wave-guiding regions resulted in improved power (>650 mW) at 80 K and 3.8 μm.[11] This result was obtained using an 808 nm diode stack pump laser, a 2 % duty cycle with 50 μsec pulses. The temperature behavior for this laser is illustrated in Figure 6(a) and (b). The lower T_0 (17 K) is most likely due to the increased duty cycle and pump laser characteristics used in this experiment.

We have recently demonstrated InAsSb/InAsP SLS injection lasers at 3.4 μm and 180 K. Under pulsed operation, peak power levels of 100 mW/facet (average power of 0.5 mW/facet) could be obtained at 80 K. A characteristic temperature (T_0) of 39 K was observed. We speculate that injection and transport of carriers in the SLS is presently limiting the performance of these devices.

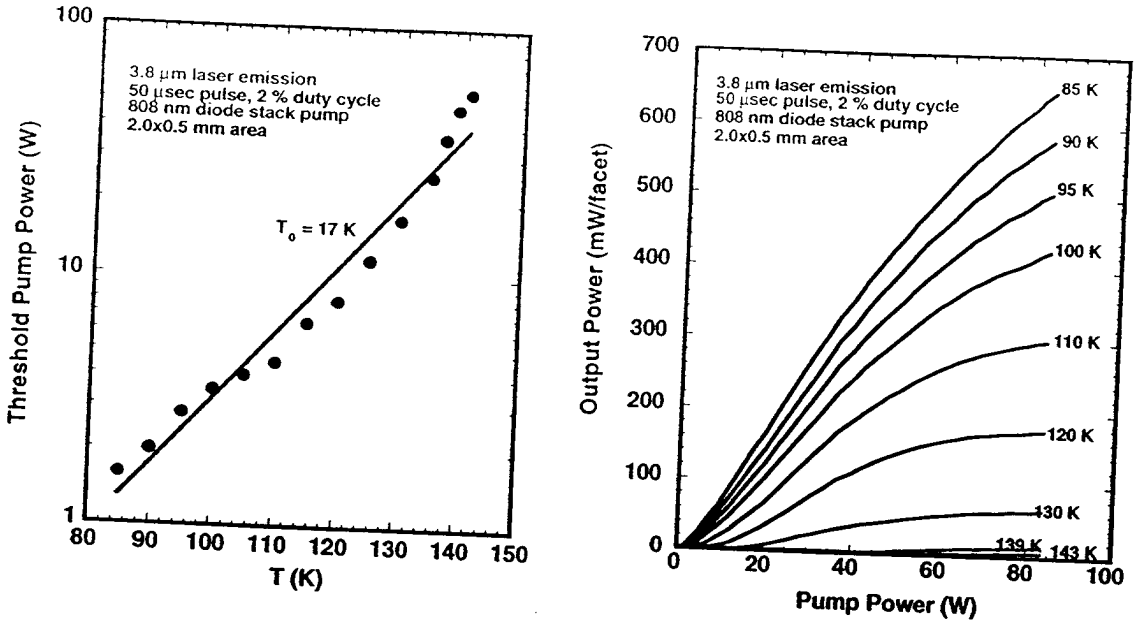

Figure 6. (a) Threshold optical pump power versus temperature. (b) Pulsed laser emission output power versus optical pump power for various temperatures for a 50 period $InAs_{0.84}Sb_{0.16}$ /$InAs_{0.68}P_{0.32}$(83 Å / 87 Å) SLS active region with 2000 Å InAs waveguides and 2 μm AlAsSb claddings.

10-Stage, Cascaded InAsSb Quantum Well Laser at 3.9 μm

We have prepared multi-stage, cascaded InAsSb quantum well lasers that lase at 3.9 μm at 170 K. The gain region of our laser was composed of 10 stages. Each stage consisted of a $GaAs_{0.09}Sb_{0.91}$ (p, 300 Å) /InAs (n, 500 Å) semi-metal , 3 $InAs_{0.85}Sb_{0.15}$ (n, 94 Å) quantum wells separated by 4 $InAs_{0.67}P_{0.33}$ (n, 95 Å) barriers, an $AlAs_{0.16}Sb_{0.84}$ (p, 50 Å) electron block, a compositionally graded, Zn-doped AlGaAsSb (p = 5 x 10^{17} cm^{-3} , 300 Å) layer and a final 50 Å, Zn-doped $GaAs_{0.09}Sb_{0.91}$ layer. The total thickness of the gain region is 1.9 μm. The excellent crystalline quality of a similar laser structure (5 quantum wells instead of 3) is demonstrated in the x-ray diffraction spectrum where groups of satellite peaks corresponding to a gain-stage period of 2100 Å and the InAsSb/InAsP period of 190 Å are observed as illustrated in Figure 7. The composition and layer thickness for the InAsSb/InAsP superlattice can be determined from the satellites with the large repeat distance where the smaller repeat distance as shown in the inset is determined by the 10-stage structure.

Optical confinement is provided by 2 μm thick , Zn-doped $AlAs_{0.16}Sb_{0.84}$ (p=1 x $10^{17}cm^{-3}$) claddings on both sides of the active region. A top 1500 Å Zn-doped $GaAs_{0.09}Sb_{0.91}$ layer (p=2 x 10^{18} cm^{-3}) is used as a contact and protective layer. The Zn doping levels were determined from Van der Pauw/Hall measurements and confirmed by secondary ion mass spectroscopy (SIMS) on thick calibration samples. Two orders of magnitude higher DEZn levels were required to obtain equivalent dopant levels in $AlAs_{0.16}Sb_{0.84}$ compared to $GaAs_{0.09}Sb_{0.91}$. This indicates a possible depletion reaction between DEZn and EDMAA. The structure is lattice matched to the InAs substrate. An InAs (n, 500 Å) /$GaAs_{0.09}Sb_{0.91}$ (p, 1000 Å) semi-metal is used to enable carrier transport from the n-type InAs substrate into the p-type $AlAs_{0.16}Sb_{0.84}$ cladding layer.

Lasing was observed from gain-guided stripe lasers. The facets were uncoated, and stripes were indium soldered to the heat sink with the epitaxial side up. Under pulsed operation with 100 nsec pulses at 1 kHz (10^{-4} duty-cycle), stimulated emission was observed from 80-170 K. Laser

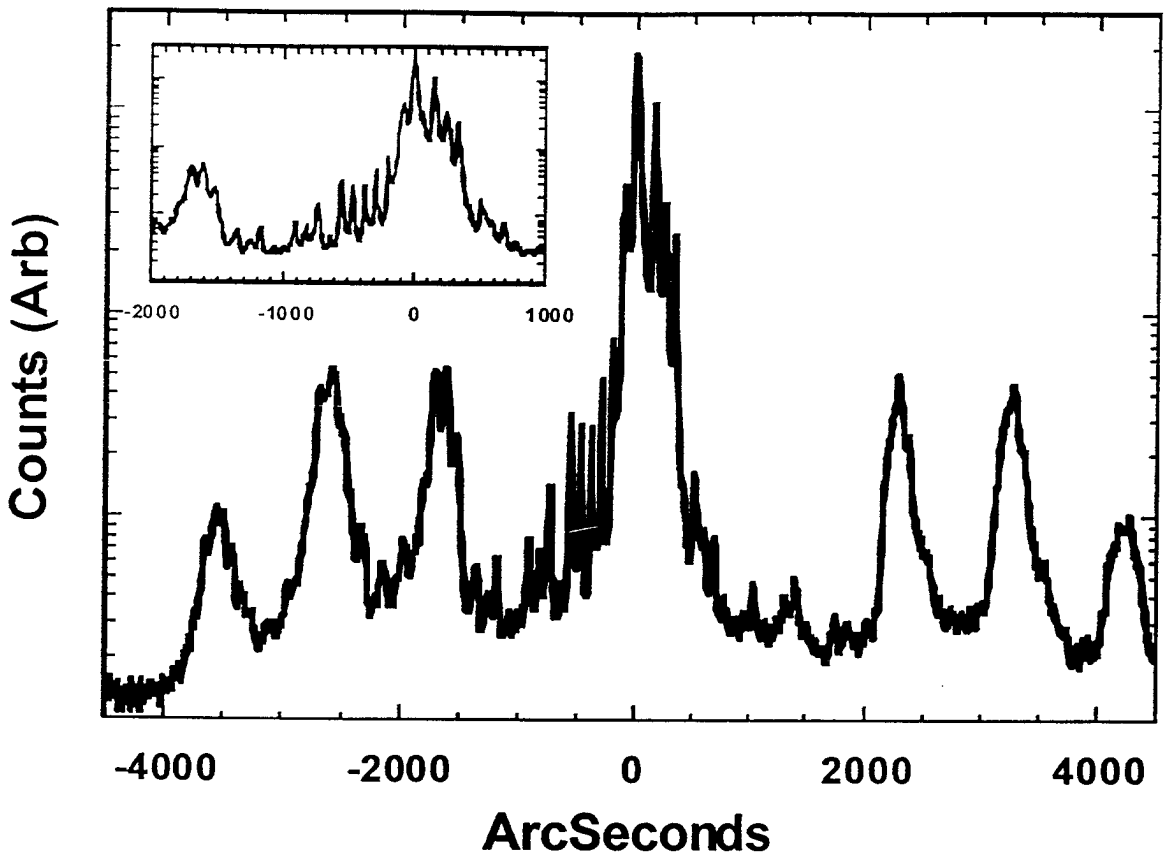

Figure 7. X-ray diffraction pattern for a 10-stage, 5-well InAsSb/InAsP laser structure with 2 μm AlAsSb claddings and p-GaAsSb/n-InAs semi-metal heterojunction injection layers.

emission spectra at 80 K and 160 K are shown in Figure 8. Emission occurred at 3.8-3.9 μm. For 750 μm long stripes with 80 μm wide metalizations, several longitudinal modes are observed with a mode spacing of 1.7 cm^{-1}. The longest laser pulses were 1 μsec. These initial devices were easily damaged by increased heating associated with higher temperature operation or longer duty cycles. Threshold current densities for these 10-stage devices were ≥ 1 kA/cm^2. Although these values are over-estimates due to current spreading in our gain-guided structures, reduction of threshold current density has not yet been demonstrated in type I or type II cascaded interband lasers.[9] Lower threshold current densities (0.1 kA/cm^2) have been demonstrated in single-stage, type I mid-infrared lasers at 80 K.[12] The characteristic temperature of a similar laser was about 34 K similar to our previously reported optically pumped InAsSb/InAsP lasers.[2]

The laser output was collected and focused directly onto an InSb detector to obtain power-current data shown in Figure 9 for the 750 μm stripe device. At 80 K, peak power values > 100 mW were obtained. At 80 K, the threshold current density was 1 kA/cm^2. The maximum slope-efficiency was 93 mW/A, corresponding to a differential external quantum efficiency of 29 % (2.9 % per stage). These slope-efficiencies are under-estimates due to current spreading in the gain-guided structures. This initial result is promising when compared to the value obtained for a second generation, 23-stage type II cascaded laser (3.9 μm) with a differential quantum efficiency of 131% (5.7 % per stage).[9]

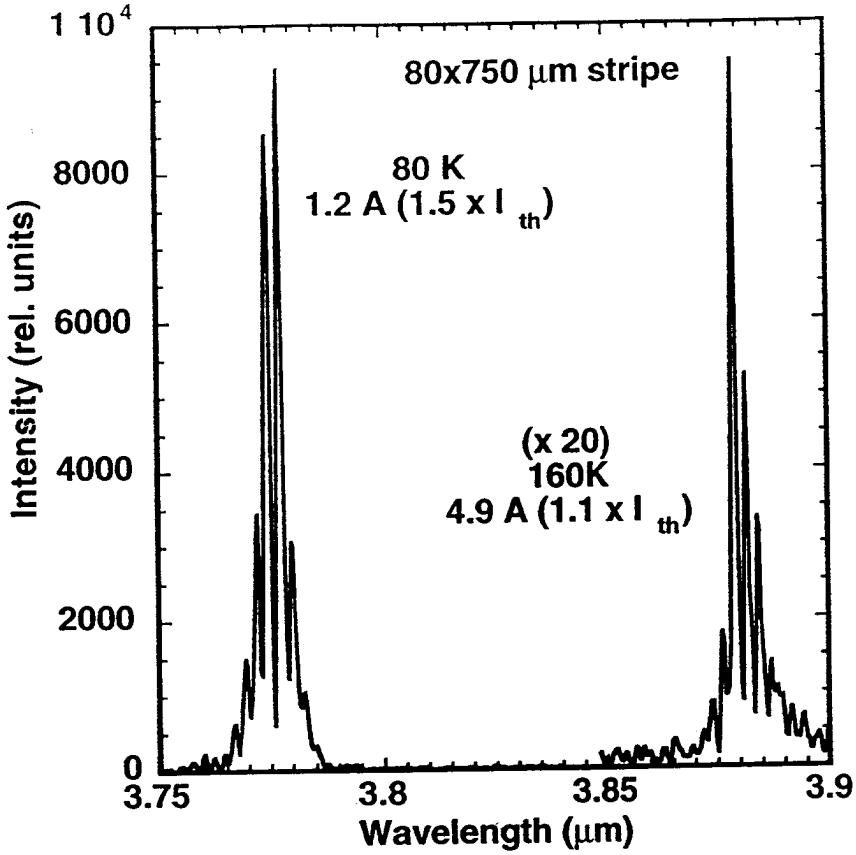

Figure 8. Laser emission spectra at 80 and 160 K for a 10-stage, 3-well laser with a 750 μm long stripe.

SUMMARY

In conclusion, we have demonstrated the first cascaded lasers and LEDs with type I InAsSb quantum well active regions. Also, these are the first cascaded devices grown by MOCVD. The 10-stage, 3.8-3.9 μm laser operated up to 170 K. At 80 K, peak laser power > 100 mW and a slope-efficiency of 29% (2.9% per stage) were observed. We are optimistic that advances in material quality and device design will improve carrier confinement and reduce loss, leading to higher efficiencies and higher temperature operation of cascaded InAsSb lasers.

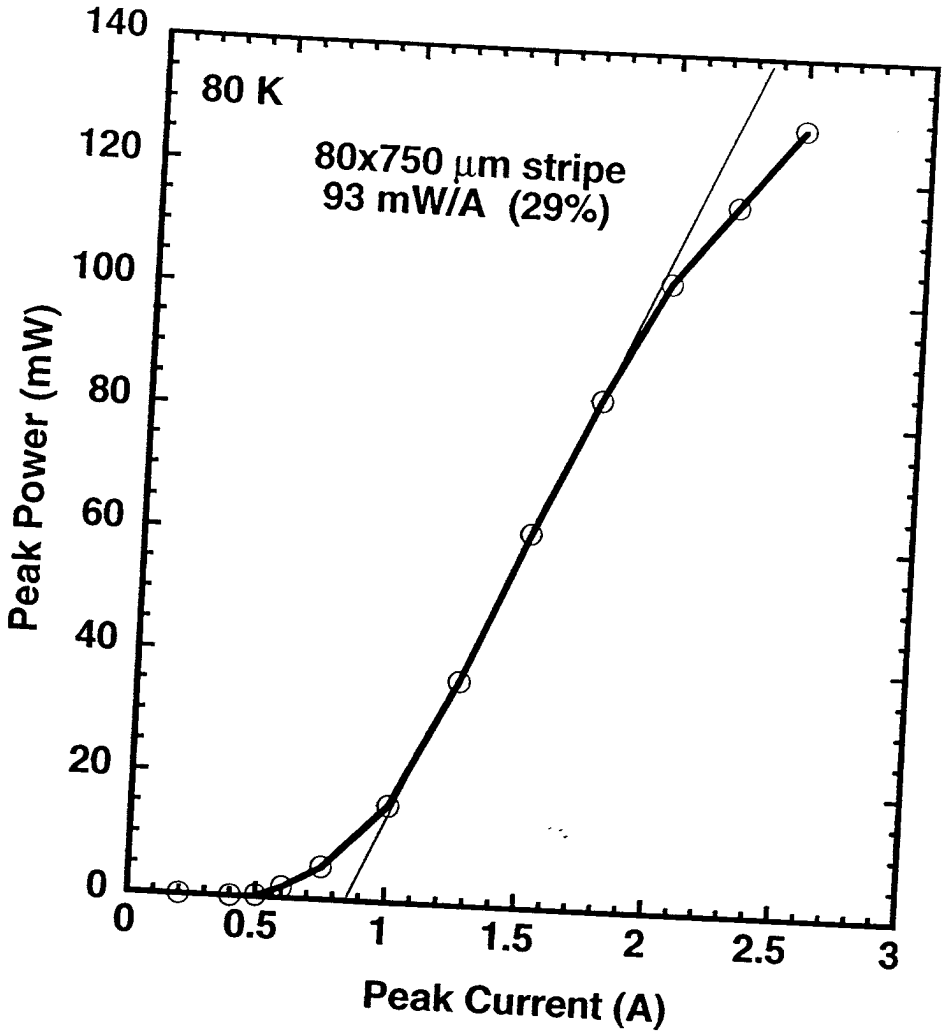

Figure 9. Peak laser power versus current for a 10-stage InAsSb/InAsP/AlAsSb/GaAsSb/InAs laser with a 750 μm long stripe at 80 K.

ACKNOWLEDGMENTS

We thank D. McDaniel of the USAF Phillips Laboratory for the results illustrated in Figure 6 and J. A. Bur and J. Burkhart for technical assistance. This work was supported by the U.S. Dept. of Energy under contract No. DE-AC04-94AL85000. Sandia is a multiprogram laboratory operated by Sandia Corporation, a Lockheed Martin Company, for the United States Department of Energy.

REFERENCES

[1] A. A. Allerman, R. M. Biefeld, and S. R. Kurtz, Appl. Phys. Lett. **69**, 465 (1996).
[2] S. R. Kurtz, A. A. Allerman, and R. M. Biefeld, Appl. Phys. Lett. **70**, 3188 (1997).
[3] R. M. Biefeld, S. R. Kurtz, and A. A. Allerman, J. Electronic Mater., **26**, 903 (1997).

[4] J. Faist, F. Capasso, D. L. Sivco, C. Sirtori, A. L. Hutchinson, and A. Y. Cho, Science **264**, 553 (1994).
[5] R. Q. Yang, Superlatt. Microstruct. **17**, 77 (1995).
[6] J. R. Meyer, I. Vurgaftman, R. Q. Yang, and L. R. Ram-Mohan, Elect. Lett. **32**, 45 (1996).
[7] J. Faist, F. Capasso, C. Sirtori, D. L. Sivco, J. N. Baillargeon, A. L. Hutchinson, S. N. G. Chu, and A. Y. Cho., Appl. Phys. Lett. **68**, 3680 (1996).
[8] C. H. Lin, R. Q. Yang, D. Zhang, S. J. Murry, S. S. Pei, A. A. Allerman, and S. R. Kurtz, Elect. Lett. **33**, 598 (1997).
[9] R. Q. Yang, B. H. Yang, D. Zhang, C. H. Lin, S. J. Murry, H. Wu, and S. S. Pei, Appl. Phys. Lett. **71**, 2409 (1997).
[10] W. G. Breiland and G. H. Evans, J. Electrochem. Soc., **138**, 1806 (1991).
[11] Private Communication from D. McDaniel, USAF Phillips Laboratory, Albuquerque, NM.
[12] H.K. Choi and G.W. Turner, Appl. Phys. Lett. **67**, 332 (1995).

Report Number (14) SAND--97-1477C
CONF--971201--

Publ. Date (11) 199801
Sponsor Code (18) DOE/MA, XF
JC Category (19) UC-900, DOE/ER

DOE